The Silicon:Colloidal Quantum Dot Heterojunction

Silvia Masala, Valerio Adinolfi, Jon-Paul Sun, Silvano Del Gobbo, Oleksandr Voznyy, Illan J. Kramer, Ian G. Hill, and Edward H. Sargent*

Crystalline silicon (c-Si) technology dominates electronics and optoelectronics: ultralarge scale integration of integrated circuits, fast optical devices, and efficient solar panels are all established applications based on c-Si. Despite its many virtues, silicon is limited in sensing, communication, and light harvesting applications by its electronic bandgap, which does not absorb light beyond 1.1 μm. The sensitization of c-Si with infrared-sensitive materials is therefore an area of great interest. Colloidal quantum dots (CQDs) offer an infrared bandgap; however, the c-Si:CQD rectifying junction has not yet been developed. Here, we construct such a junction, but find initially that an energy band mismatch and highly defective c-Si:CQD interface prevent efficient extraction of photocurrent. We then devise a means of functionalizing the c-Si:CQD interface that simultaneously passivates the silicon and CQD terminations, and, further, introduces an interface dipole that produces a favorable band alignment between the two solids. Only by so doing are we then able to demonstrate, for the first time, efficient injection of infrared-generated (>1.1 μm absorbed photon wavelength) photocharges from the CQD layer into silicon. Our integrated c-Si:CQD photodiode achieves a high responsivity, of 0.4 A W^{-1}, for 1.23 μm incident radiation. This materials' platform, in contrast to established epitaxial approaches (Ge, III–V compounds), allows for room temperature large-area and low cost farication processes.

c-Si is widely used in photonic devices as a light-guiding medium because of its high index, low loss, and robust electronic performance. Its utility in light detection,[1,2] especially in the shorter visible wavelengths of the optical spectrum, makes it the workhorse of digital imaging today.[3,4] Unfortunately, silicon's 1.1 eV bandgap prevents it from providing photon detection in the short-wavelength infrared (SWIR), i.e., at wavelengths greater than 1.1 μm. This regime is particularly useful for night-time imaging based on atmospheric nightglow;[5] as well as

Dr. S. Masala, Dr. S. D. Gobbo
Division of Physical Sciences and Engineering
Solar and Photovoltaics Engineering Research Center
King Abdullah University of Science
and Technology (KAUST)
Thuwal 23955-6900, Saudi Arabia
V. Adinolfi, Dr. O. Voznyy, Dr. I. J. Kramer,
Prof. E. H. Sargent
Department of Electrical and Computer Engineering
University of Toronto
10 King's College Road
Toronto, Ontario, M5S 3G4, Canada
E-mail: ted.sargent@utoronto.ca
J.-P. Sun, Prof. I. G. Hill
Department of Physics and Atmospheric Science
Dalhousie University
1459, Oxford Street, Halifax, Nova Scotia, B3H 4R2, Canada

in gesture recognition, automated inspection and process quality control,[6] medical imaging,[7,8] and on-chip communications.[9]

There exist numerous prior reports of nonmonolithic (hybrid) integration onto silicon of separately epitaxially grown materials such as III–V compound semiconductors. This package-level integration increases cost and device size and often demands bonding processes incompatible with complementary metal oxide semiconductor (CMOS) technology.[10] Further, the materials comprising III–V compounds can contaminate silicon,[11] strongly affecting its electronic properties; these problems limit the potential for a facile and direct integration of III–V compounds onto silicon. Crystalline germanium has been extensively used to create heterojunction devices with c-Si, but also suffers from complexity of fabrication and a reliance on high temperature growth.[12]

Graphene:c-Si heterostructures have extended the range of light sensitivity of silicon devices to the mid-infrared, but only when combined in a waveguide structure.[13] Graphene's weak optical absorption, in the vicinity of 2% per monolayer,[14,15] requires sophisticated optical structures[16] to provide acceptable sensitivities when combined with c-Si in a diode structure. The requirement of multimicrometer interaction lengths stands in the way of applications such as imaging that require ≈1 μm pixel dimensions.

The realization of a high-performance, room-temperature-processed silicon-integrated heterojunction that is responsive beyond 1.1 um remains an unmet challenge as of this report.[17,18]

CQDs have seen rapid growth in the last decade in optoelectronics because of their room-temperature solution processing and low cost and spectral tunability.[19] This class of semiconductor solids has shown considerable promise in photovoltaics[20,21] and photodetection, including at SWIR wavelengths.[22,23] Development of a heterojunction device between a CQD solid and electronic-grade silicon would enable a monolithically integrated, tunable, and SWIR-responsive device platform.

The combination of CQDs and silicon has primarily been used to enhance absorption of structured p–n silicon solar cells in the visible range.[24] c-Si:CQD rectifying solar cells have been presented, but to date exhibit no extraction of carriers generated using subsilicon-bandgap (>1.1 μm) illumination.[25,26] The reasons for this failure of the c-Si:CQD heterointerface have, to this point, been unexplored and unexplained.

Here we investigate the c-Si:CQD monolithically integrated rectifying junction. We find that a specific and novel combination of process conditions is required to achieve the efficient collection of SWIR photogenerated charges. We then proceed to build an efficient photodetector using a room-temperature solution-processed material compatible with CMOS technology. The diode investigated here (**Figure 1**a,b) is based on a p-type silicon wafer (⟨100⟩ crystalline orientation) that we overcoat
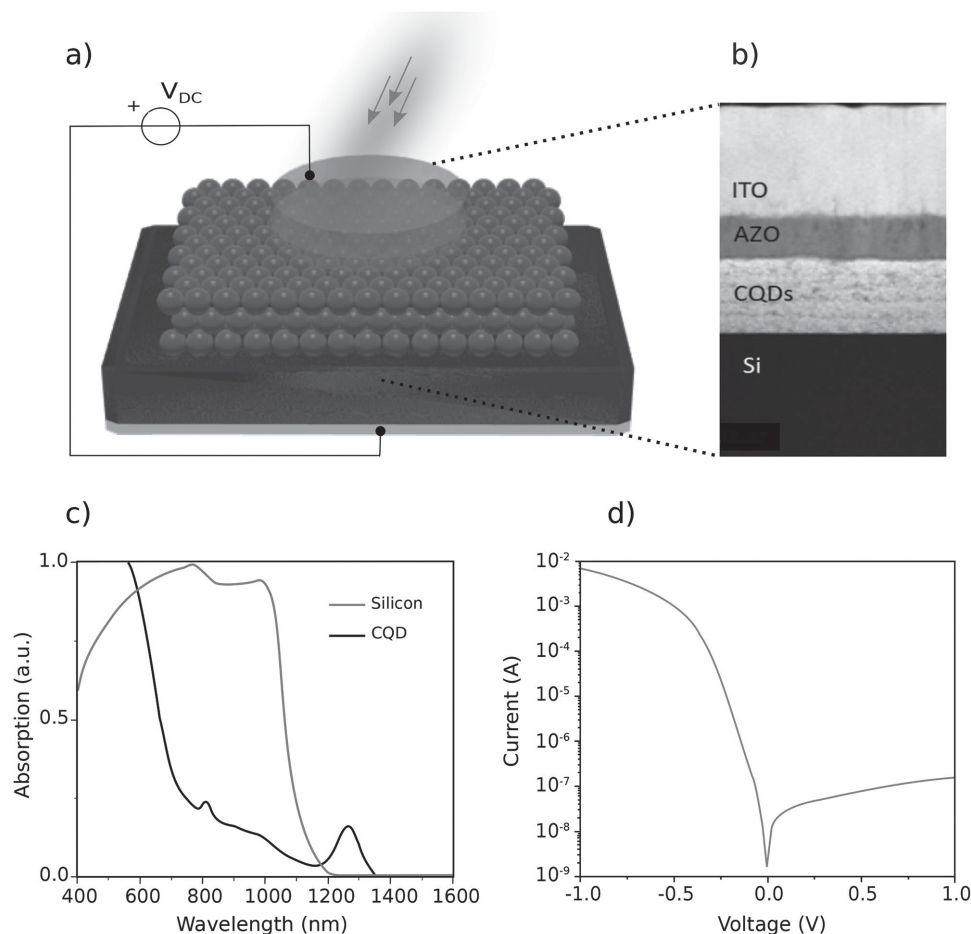
Figure 1. c-Si:CQD junction and materials properties. a) Schematic of the c-Si:CQD photodiode architecture: p-type silicon is coated with the CQD layer; the transparent (illuminated) top contact is realized with AZO and ITO; and the silicon side of the junction is contacted using aluminum on the back side. b) STEM cross-section of the diode. c) Measured absorption of c-Si and CQDs. The CQDs are characterized by an excitonic peak centered at 1230 nm. d) cSi:CQDs current–voltage plot showing rectification.

using a 150 nm film of halide-treated n-type PbS CQD (1 eV bandgap). The diode is top illuminated through a transparent metal oxide layer deposited on the CQD film. In order to collect photocharges efficiently from the CQD layer, the following three requirements must be fulfilled simultaneously:

i. The c-Si and CQDs must be in intimate contact while employing an effective passivation of interfacial defects.
ii. The band alignment of the two semiconductors must not result in an energetic barrier for the photocarriers generated in the CQD film.
iii. A depletion region supplying a built-in charge extracting electric field must extend into the CQD layer to overcome limited electric transport in this semiconductor.[27]

Simultaneously satisfying conditions (i), (ii), and (iii) should enable efficient detection of wavelengths of light inaccessible to the c-Si layer, but to which the CQD are sensitive.

We started our study using a common c-Si interface treatment, the application of hydrofluoric acid (HF) on the precleaned silicon surface. This procedure removes the native oxide covering the silicon surface and passivates superficial dangling

bonds using hydrogen.[28–30] Deposition of a CQD film on HF-treated c-Si produced a rectifying junction; however, the forward-to-reverse current ratio was undesirably low and the onset of a breakdown is seen at a small voltage of ≈6 V (see Figure S1 in the Supporting Information). We interpreted this result as evidence that condition (i) was not fully satisfied: intimate contact between silicon and CQD had been realized, but with poor passivation of the interface states, thus limiting the device performance.

Halides have been shown to be superior to hydrogen in passivating silicon surfaces;[31–33] further, halide treatments of CQD solids were recently found to result in well passivated, n-type films.[34,35] A halide surface treatment would therefore promote compatibility at the c-Si:CQD interface, and also enable a p-type c-Si:n-type CQD rectifying junction. Pursuing this route, we used iodine to modify the silicon surface chemically. Following the treatment, we investigated adsorbed iodine on the bare silicon surface using X-ray photoelectron spectroscopy (XPS) (Figures S2 and S3, Supporting Information). The c-Si:CQD diode built using this passivation technique showed improved rectification compared to the HF-treated device (Figure 1d; Figure S1, Supporting Information); its reverse saturation current was fully one order of magnitude lower. An

accompanying elimination of low-voltage device breakdown was also observed. Using the transient photoconductance decay technique[36] (Table S1, Supporting Information), we measured charge carrier lifetime and confirmed that the improved rectification arose from a reduced trap state density in iodine-passivated samples compared to HF acid-passivated samples. The carrier lifetime is inversely proportional to the density of traps and therefore is an indicator of interface passivation.

While impressive rectification was achieved by satisfying requirement (i), spectral external quantum efficiency (EQE) measurements clearly indicated the lack of photocurrent collected from the CQD layer, i.e., beyond 1.1 μm (Figure S4, Supporting Information). We therefore proceeded to analyze the energy band alignment of the heterojunction to see if it was limiting the extraction of photocharges from the CQD layer (requirement (ii)). In **Figure 2**a, the energy diagram of the junction is drawn according to the Anderson rule for the electron affinities.[37] Published conduction and valence band energies were used for c-Si while the energetic picture of the CQD film was determined by cyclic voltammetry and optical absorption measurements (Figure S5,

Supporting Information). The c-Si:CQD band lineup resulting from this model produces a type-I heterojunction (Figure 2a) with an undesired barrier of 0.09 eV in the valence band. This blocks the flow of photoholes from the CQDs to the silicon. This barrier prevents the new diode from sensing radiation beyond 1.1 μm.

By adding a dipole to the interface between the c-Si surface and the CQD film, we can realize the efficient collection of photocharges across the c-Si:CQD boundary.[38] Chemisorbed molecular species can form surface dipoles to tune the work function of metals and semiconductors.[39] In the energy diagram, the dipole introduces a discontinuity of the vacuum level ΔE_{vac} at the interface (Figure 2b) that modifies the band alignment of the junction. In light of the success in passivating the interface achieved by the I_2 treatment, we screened other halide and organohalide compounds such as bromide (Br_2) and methyl iodide (CH_3I). Each of these chemical compounds has been used on c-Si surfaces, resulting in Si–Br and Si–CH_3 and Si–I bonds, respectively.[40–42] We analyzed the energetic alignment at the silicon surface for all the three interface treatments using established techniques, particularly UPS and Kelvin probe measurements.[43–47] These
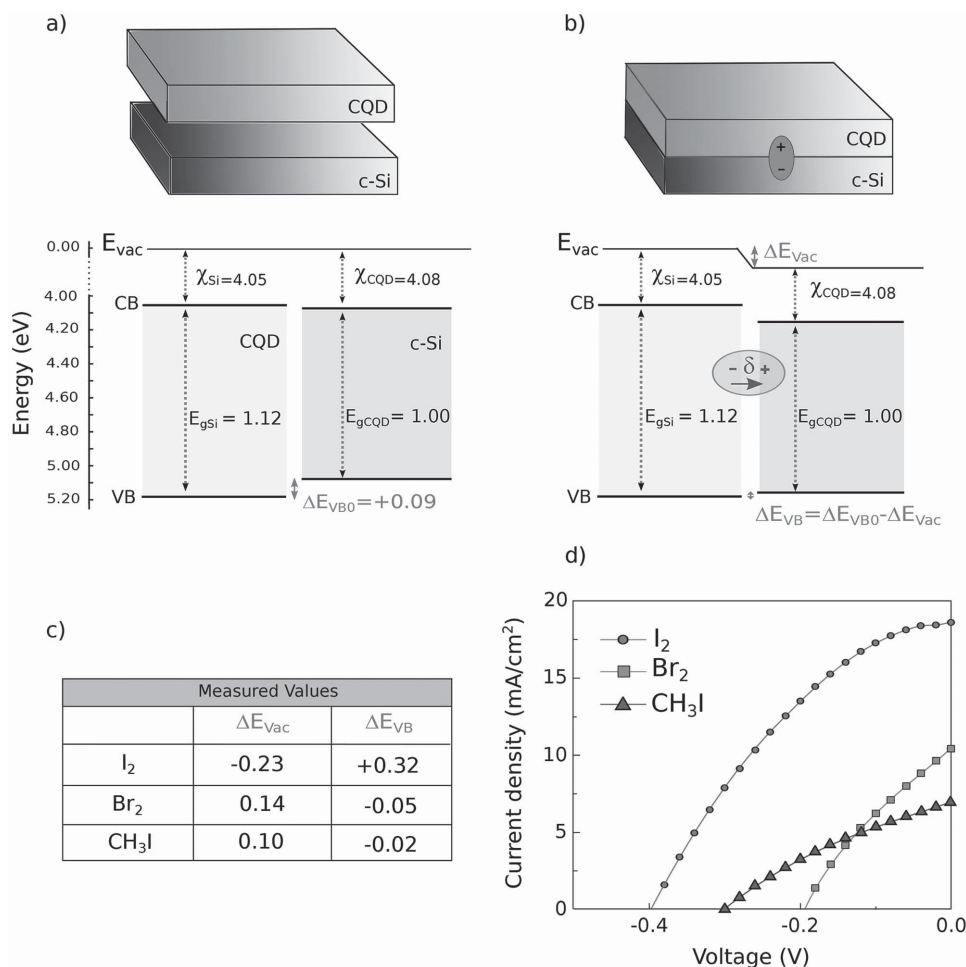

Figure 2. Schematic of the effect of surface dipole on c-Si energy band and current density–voltage (J–V) characteristics under 100 mW cm^{-2} AM 1.5 light. Energy diagram of the c-Si:CQDs diode a) without and b) with the effect of the interface dipole. The dipole introduces a discontinuity ΔE_{vac} in the vacuum level at interface. c) Vacuum level offset ΔE_{vac} and valence band offset ΔE_{VB} as measured from UPS and Kelvin Probe measurements for different halogen treatment of the silicon. d) Experimental J–V curves for each c-Si:CQD device.

methods (Figure S8, Supporting Information) revealed the presence of a different dipole moment for each of the surface engineering approaches. The results are summarized in Figure 2c. Specifically, a measured $\Delta E_{vac} = +0.23 \pm 0.04$ eV corresponding to a valence band offset $\Delta VB = +0.32 \pm 0.04$ eV on I_2-terminated silicon confirms the presence of the energetic barrier for holes (**Figure 3**a). Further analysis of the experimental data reveals that the dipole moment formed by adsorbed Br_2 and CH_3I nullifies ΔVB at the c-Si:CQD interface, thereby simultaneously satisfying requirements (i) and (ii). Efficient collection of photogenerated charges from the CQD film is therefore expected in the case of CH_3I and Br_2-treated silicon diodes.

To verify this prediction, we measured the current–voltage (*I–V*) characteristics under AM 1.5 illumination for diodes with the dipole treatments applied (Figure 2d). All halide treatments show significant short-circuit photocurrent and open circuit voltage (V_{OC}). We note that the relation between the three V_{OC} is in agreement with the energetic landscapes previously depicted: the iodine-treated diodes exhibited the highest V_{OC} of 0.40 V whereas the V_{OC} of CH_3I and Br_2 diodes was reduced to 0.30 and 0.19 V respectively. This trend is consistent with the direction of the dipole moment formed at the chemically treated c-Si surface and therefore the changes occur in band alignment between the p-type c-Si and the n-type CQDs.

Carrier lifetime measurements confirmed that all three halide surface treatments significantly reduce trap density compared to HF treatment. In particular, I_2 and CH_3I treatments show a significant enhancement while the Br_2 only slightly improves over HF (Table S1, Supporting Information).

We then investigated the spectral contributions to the photocurrent (EQE) for the three halide-treated c-Si:CQD diodes

(Figure 3). These results were further validated using optoelectronic simulations[48] (dashed line in Figure 3a–c). Beneath each EQE plot, the corresponding energy band diagram, simulated in the short-circuit condition, is presented (Figure 3d–f).

The EQE spectrum for the I_2-treated diode shows the collection of charges photogenerated (mostly due to visible light absorption) within the silicon; the bluer wavelengths are largely absorbed in the CQDs, as are the >1.1 um wavelengths, and as a result these photocarriers are uncollected in light of the valence band barrier from CQDs to silicon.

The spectral response of Br_2-treated diodes exhibits a notable contribution to photocurrent from the CQDs, particularly beyond 1100 nm, where silicon is transparent to photons. As shown in the energy diagram, the interface dipole ensures that no appreciable barrier in the valence band stands in the way of photohole egress from the CQD side into the cSi. Despite this important result, the carrier collection efficiency is reduced at all wavelengths compared to the I_2 case previously discussed. We attributed the overall low EQE to the low built-in voltage (see the band alignment for Br_2 treatment in Figure 2) that produces only minimal band bending in the CQD film, limiting photohole transport therein.

The CH_3I-treated heterojunction shows the highest EQE in the SWIR spectral region with 14% EQE at 1.23 μm. This indicates the fulfillment of the three requirements: interface passivation, proper band alignment, and a depleted CQD layer. We note a reduced contribution to the spectral response coming from the silicon layer that we can explain if we posit acceptor states at the interface. These states decrease the flux of photoelectrons from the silicon side into the CQD solid. The accumulation of negative charge at the interface is offset by an
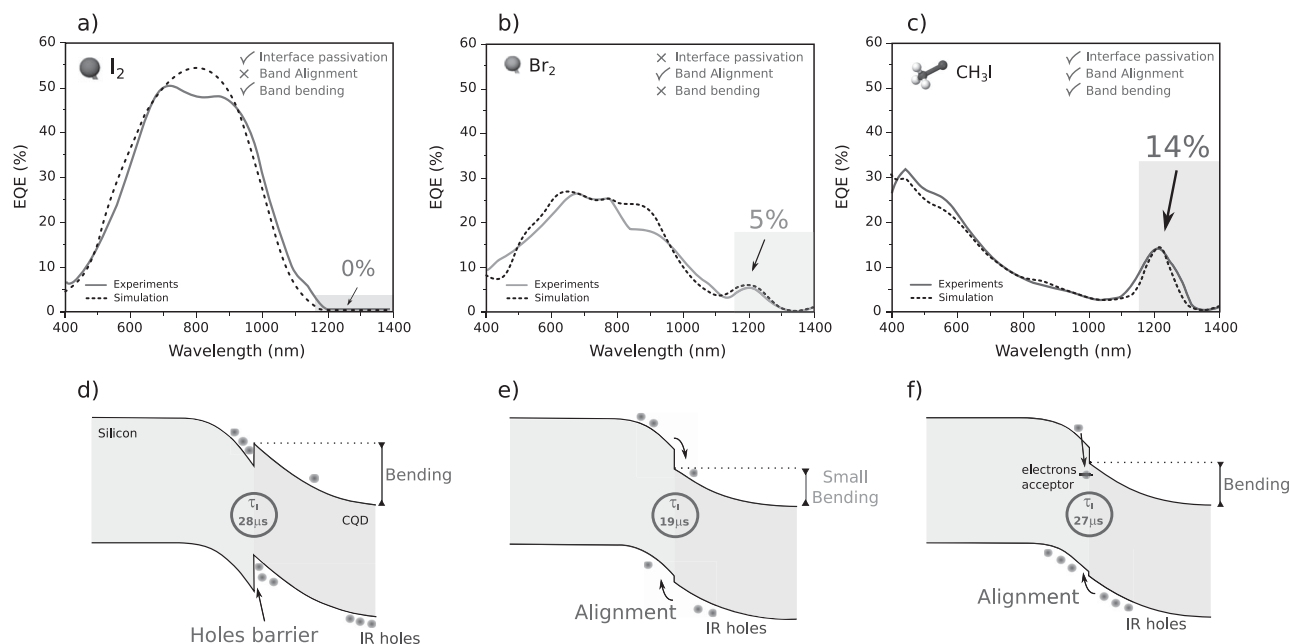

Figure 3. Spectral photoresponse of c-Si:CQD heterojunction diodes. a,b,c) Measured (solid line) and simulated (dashed line) Spectral EQE different halogen treatments: a) I_2, b) Br_2, c) CH_3I. d–f) Energy band diagram at short-circuit condition, under 100 mW cm^{-2} AM 1.5 solar illumination and interface carrier lifetime (at the center of each diagram) for each diode: d) I_2, e) Br_2, and f) CH_3I. Ideal band alignment is achieved in the case of CH_3I and Br_2 treatment while I_2-treated devices exhibit a valence band offset (0.32 eV) blocking holes generated in the CQD layer. The band bending in the CQD layer varies according to band alignment (built-in potential) and is reduced proceeding from the I_2-devices to the CH_3I- and Br_2-treated ones.
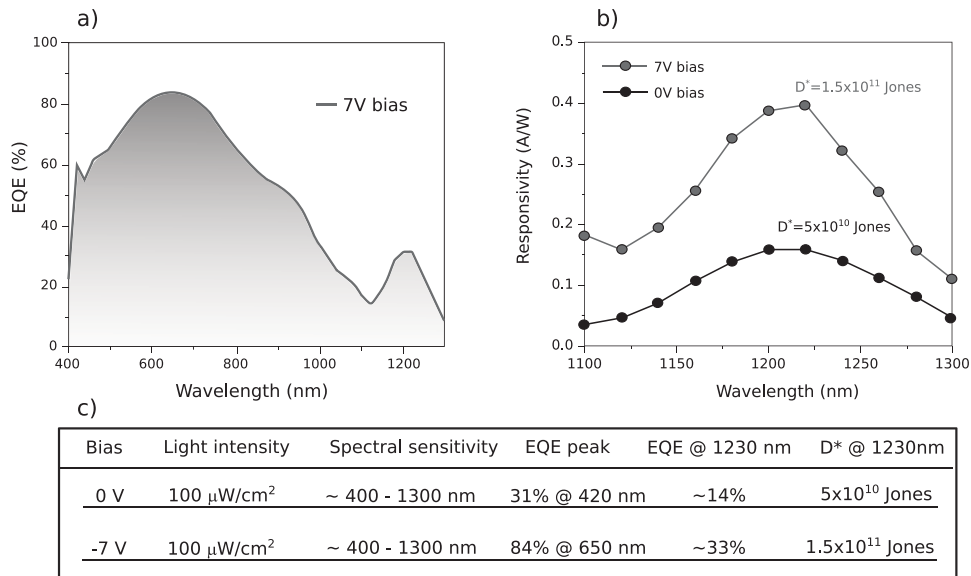
Figure 4. Spectral responsivity and detectivity of c-Si:CQD photodiodes. a) Spectral EQE recorded at 7 V reverse bias on a CH_3I-treated photodiode. b) Responsivity measured at 0 V and 7 V reverse bias under 100 µW cm^{-2} power. The detectivity was calculated at 1.236 µm, the CQD exciton absorption peak. c) Table summarizing the figures of merit of the detector at different bias conditions.

increased depletion region in the CQD semiconductor, and this enhances extraction of CQD-absorbed photoholes especially apparent at UV and IR wavelengths.

Using the best-performing CH_3I treatment, we fabricated and characterized the first monolithically integrated c-Si:CQD photodetector. The EQE at 1236 nm, under an applied reverse bias of 7 V, reaches 33%, corresponding to a responsivity of 0.4 A W^{-1} (**Figure 4**a,b). The specific detectivity of the photodiode at 1236 nm $D^* = \dfrac{R\sqrt{A}}{\sqrt{2qI_{dark}}}$ where A is the area of the device (0.049 cm^2), q is the electron charge, R is the responsivity, and I_{dark} is the dark current) is $D^* = 1.5 \times 10^{11}$ Jones. Under reverse bias, the spectral response presents contributions also from the silicon layer, overcoming 80% EQE in the visible range. This responsivity is competitive with that of epitaxial germanium-on-silicon photodetectors. Additionally the device offers a several order-of-magnitude improvement of dark current density.[12] These attractive performance enhancements come without the need for epitaxy. The fabrication of the detector herein is executed at room temperature and is CMOS compatible. The responsivity of the detector is expected to be a weak function of the incident light power as observed previously in CQD[49] and Si photodiodes.

In conclusion, the fabrication of a c-Si:CQD heterojunction for SWIR sensitization of c-Si allowed us to expand the spectral operating range of silicon-based devices. We overcame the limits arising from the natural band alignment of c-Si and CQDs that previously prevented the realization of efficient devices. We did so by using a judicious choice of c-Si surface chemical treatment that also offered the needed CQD type and performance. We further engineered the band alignment and enabled the emergence of a strong built-in electric field. By satisfying three critical operating requirements, we demonstrated the first CQD photodetector monolithically integrated with c-Si to exhibit responsivity beyond silicon's bandgap.

Experimental Section

Silicon Cleaning and Surface Treatment: The silicon wafers were cleaned according to the standard RCA cleaning procedure to remove organic and metal contaminants. First, the wafer was dip in a solution of ammonium hydroxide:hydrogen peroxide:deionized water at ratio 1:1:5 at 80 °C for 15 min (RCA 1). Then, it was rinsed in DI water and immersed in oxide stripping solution made of 2% hydrofluoric acid (HF). Finally, the wafer was cleaned in hydrochloric acid:hydrogen peroxide:deionized water at ratio 1:1:5 at 80 °C for 15 min (RCA 2).

Before the halogenation, the wafer surface was etched with a solution of 2% HF, rinsed in DI water for 30 to 60 s to avoid formation of new oxide, and transferred in a nitrogen filled glove box ($O_2 < 2$ ppm) for the subsequent surface treatment. *Iodine Treatment*: The wafer was sealed in a petri dish with a few milligrams of solid iodine and heated up for 20 min. *Methyl Iodine Treatment*: The wafer was dipped in a solution of CH_3I in diethyl ether and exposed to ultraviolet light (254 nm) for 20 min. *Bromine Treatment*: The wafer was exposed to bromine vapor at room temperature by sealing it in a petri dish containing a few microliters of bromine in liquid phase.

CQD Film Deposition and Device Fabrication: PbS CQDs dispersed in octane were deposited layer by layer on the c-Si wafer by spin casting. The layer was made n-type doped by replacing the original long oleic acid ligands of the CQDs with atomic size inorganic ones coming from tetrabutyl ammonium iodide (TBAI). During the solid state treatment a solution of TBAI in methanol, 10 mg mL^{-1} was dispensed after each layer and spun dry after 30 s at 2500 rpm for 10 s. Then two rinses with methanol were done at the same speed. The top metal oxide contact was deposited by sputtering at base pressure of 5×10^7 Torr. It consisted of 30 nm thick of 2% aluminum-doped zinc oxide (AZO), which is an ohmic contact with the n-type film and 200 nm thick indium tin oxide (ITO) layer added to reduce sheet resistance. The back contact was made of Al and deposited by thermal evaporation on the back, not polished, side of the wafer after RCA cleaning process and oxide stripping. The Al layer thickness was 150 nm. Post metallization annealing was performed at 450 °C for 15 min in nitrogen. The device area, 0.049 cm^2, was defined on the top layer through a shadow mask.

Absorption measurements were carried out using a Cary 500 UV–vis–IR spectrometer in an integrating sphere.

ADVANCED
MATERIALS
www.advmat.de

Materials Views
www.MaterialsViews.com

COMMUNICATION

I–V and EQE Characterization: I–V curves were recorded using a Keithley 2400 digital multimeter. The spectral EQE measurements were carried out using a 400W Xenon lamp (Horiba Jobin-Yvon), a monochromator (Horiba JobinYvon FL-1039) optical filter (Newport), and an optical chopper operating at 200 Hz. The chopper was coupled with a Stanford Research Systems lock-in amplifier, which was used to measure the photogenerated current. The collimated light was measured through a 0.049 cm^2 aperture using a calibrated Newport 818-UV and Newport 818-IR power meters.

Electrooptical Model: Device modeling was performed using SCAPS, a 1D solar cell simulation program developed at the department of Electronics and Information Systems (ELIS) of the University of Gent, Belgium.

Supporting Information

Supporting Information is available from the Wiley Online Library or from the author.

[1] R. Soref, L. Fellow, I. Paper, *Sel. Top. Quantum Electron. IEEE J.* **2012**, *12*, 1678.

[2] L. Pavesi, D. J. Lockwood, *Silicon Photonics*. Vol. *94*, Springer, Berlin **2004**.

[3] R. A. Soref, *Silicon-Based Optoelectronics. Proc. IEEE* **1993**, *81*, 1687.

[4] G. Masini, L. Colace, G. Assanto, *Mater. Sci. Eng. B* **2002**, *89*, 2.

[5] G. Konstantatos, I. Howard, A. Fisher, S. Hoogland, J. Clifford, E. Klem, L. Levina, E. Sargent, *Nature* **2006**, *442*, 180.

[6] M. P. Hansen, D. S. Malchow, in *SPIE Def. Secur. Symp.*, Vol. *6939* (Eds: V. P. Vavilov, D. D. Burleigh) International Society for Optics and Photonics, Baltimore, USA **2008**, pp. 693901–11.

[7] Y. T. Lim, S. Kim, A. Nakayama, N. E. Stott, N. G. Bawendi, J. V. Frangioni, *Mol. Imaging* **2003**, *2*, 50.

[8] S. Kim, Y. T. Lim, E.G. Soltesz, A. M. De Grand, J. Lee, A. Nakayama, J. A. Parker, T. Mihaljevic, R. G. Laurence, D. M. Dor, L. H. Cohn, M. G. Bawendi, J. V. Frangioni, *Nat. Biotechnol.* **2004**, *22*, 93.

[9] S. Luryi, A. Kastalsky, J. C. Bean, *IEEE Trans. Electron Devices* **1984**, *31*, 1135.

[10] K. Tanabe, K. Watanabe, Y. Arakawa, *Sci. Rep.* **2012**, *2*, 349.

[11] J. Wang, S. Lee, *Sensors* **2011**, *11*, 696.

[12] J. Michel, J. Liu, L. C. Kimerling, *Nat. Photonics* **2010**, *4*, 527.

[13] X. Wang, Z. Cheng, K. Xu, H. K. Tsang, J.-B. Xu, *Nat. Photonics* **2013**, *7*, 1.

[14] F. Xia, T. Mueller, Y.-M. Lin, A. Valdes-Garcia, P. Avouris, *Nat. Nanotechnol.* **2009**, *4*, 839.

[15] R. R. Nair, P. Blake, A. N. Grigorenko, K. S. Novoselov, T. J. Booth, T. Stauber, N. M. R. Peres, A. K. Geim, *Science* **2008**, *320*, 1308.

[16] S. Thongrattanasiri, F. H. L. Koppens, F. J. García De Abajo, *Phys. Rev. Lett.* **2012**, *108*, 047401.

[17] M. Streshinsky, R. Ding, Y. Liu, A. Novack, Y. Yang, Y. Ma, X. Tu, E. K. S. Chee, A. E.-J. Lim, P. G.-Q. Lo, T. Baehr-Jones, M. Hochberg, *Opt. Photonics News* **2013**, *24*, 32.

[18] T. Baehr-Jones, T. Pinquet, P. LoGuo-Quiang, S. Danziger, D. Prather, M. Hochberg, *Nat. Photonics* **2012**, *6*, 206.

[19] J. Y. Kim, O. Voznyy, D. Zhitomirsky, E. H. Sargent, *Adv. Mater.* **2013**, *25*, 4986.

[20] J. Tang, E. H. Sargent, *Adv. Mater.* **2011**, *23*, 12.

[21] E. H. Sargent, *Nat. Photonics* **2012**, *6*, 133.

[22] G. Konstantatos, E. H. Sargent, *Infrared Phys. Technol.* **2011**, *54*, 278.

[23] J. P. Clifford, G. Konstantatos, K. W. Johnston, S. Hoogland, L. Levina, E. H. Sargent, *Nat. Nanotechnol.* **2009**, *4*, 40.

[24] H.-C. Chen, C.-C. Lin, H.-W. Han, Y.-L. Tsai, C.-H. Chang, H.-W. Wang, M.-A. Tsai, H.-C. Cuo, P. Yu, *Opt. Express* **2011**, *19*, A1141.

[25] C.-Y. Huang, D. Y. Wang, Y. T. Wang, Y. T. Jiang, Y. J. Jiang, C. C. Chen, Y. F. Chen, *J. Phys. D. Appl. Phys.* **2011**, *44*, 085103.

[26] T. Song, F. Zhang, X. Lei, Y. Xu, S. Lee, B. Sun, *Nanoscale* **2012**, *4*, 1336.

[27] Z. Ning, D. Zhitomirsky, V. Adinolfi, B. Sutherland, J. Xu, O. Voznyy, P. Maraghechi, X. Lan, S. Hoogland, Y. Ren, E. H. Sargent, *Adv. Mater.* **2013**, *25*, 1719.

[28] G. Trucks, K. Raghavachari, G. Higashi, Y. Chabal, *Phys. Rev. Lett.* **1990**, *65*, 504.

[29] K. J. Chang, D. J. Chadi, *Phys. Rev. Lett.* **1988**, *60*, 1422.

[30] E. Yablonovitch, D. L. Allara, C. C. Chang, T. Gmitter, T. B. Bright, *Phys. Rev. Lett.* **1986**, *57*, 249.

[31] A. G. Aberle, *Prog. Photovoltaics Res. Appl.* **2000**, *8*, 473.

[32] T. S. Horányi, T. Pavelka, P. Tüttö, *Appl. Surf. Sci.* **1993**, *63*, 306.

[33] H. M'saad, J. Michel, J. J. Lappe, L. C. Kimerling, *J. Electron. Mater.* **1994**, *23*, 487.

[34] D. Zhitomirsky, M. Furukawa, J. Tang, P. Stadler, S. Hoogland, O. Voznyy, H. Lu, E. H. Sargent, *Adv. Mater.* **2012**, *24*, 6181.

[35] Z. Ning, Y. Ren, S. Hoogland, O. Voznyy, L. Levina, P. Stadler, X. Lan, D. Zhitomirsky, E. H. Sargent, *Adv. Mater.* **2012**, *24*, 6295.

[36] R. A. Sinton, A. Cuevas, M. Stuckings, presented at Conf. Rec. Twenty Fifth IEEE Photovolt. Spec. Conf. 1996, IEEE, Washington, DC, May **1996**.

[37] R. L. Anderson, *Solid. State. Electron.* **1962**, *5*, 341.

[38] J. Tersoff, *Phys. Rev. B* **1984**, *30*, 4874.

[39] Y. Zhou, C. Fuentes-Hernandez, J. Shim, J. Meyer, A. J. Giordano, H. Li, *Science* **2012**, *336*, 327.

[40] M. L. Colaianni, P. J. Chen, H. Gutleben, J. Yates, T. Vibrational, *Chem. Phys. Lett.* **1992**, *191*, 561.

[41] M. J. Kong, S. S. Lee, J. Lyubovitsky, S. F. Bent, *Chem. Phys. Lett.* **1996**, *263*, 1–7.

[42] N. Batra, Vandana, S. Kumar, M. Sharma, S. K. Srivastava, P. Sharma, P. K. Singh, *Sol. Energy Mater. Sol. Cells* **2012**, *100*, 43–47.

[43] T. Kitatani, M. Kondow, T. Kilkawa, Y. Yazava, M. Okai, K. Uomi, *Jpn. J. Appl. Phys.* **1999**, *38*, 5003–5006.

[44] L. Chkoda, C. Heske, M. Sokolowski, E. Umbach, F. Steuber, J. Staudigel, M. Stobel, J. Simmerer, *Synth. Met.* **2000**, *111–112*, 315–319.

[45] T. Mizutani, T. Usunami, S. Kishimoto, K. Maezawa, *Jpn. J. Appl. Phys.* **1999**, *38*, L767–L769.

[46] M. Tanimoto, *J. Vac. Sci. Technol. B Microelectron. Nano. Struct.* **1996**, *14*, 1547.

[47] J. R. Waldrop, R. W. Grant, *Appl. Phys. Lett.* **1996**, *68*, 2879.

[48] M. Burgelman, P. Nollet, S. Degrave, *Thin Solid Films* **2000**, *361-362*, 527–532.

[49] J. P. Clifford, G. Konstantatos, K. W. Johnston, S. Hoogland, L. Levina, E. H. Sargent, *Nat. Nanotechnol.* **2009**, *4*, 40–44.